

Design of curved photonic cavities for a narrow-band widely tunable resonance ranging 200 nm

Guanquan Liang,* Aaron J. Danner, and Chengkuo Lee

Department of Electrical and Computer Engineering, National University of Singapore 117576, Singapore
elegq@nus.edu.sg

Abstract: We propose a type of photonic resonator with a tunable curved cavity that enables efficient tuning of the optical length of a resonant cavity made of a solid material; we call this a “tunable curved resonator” (TCR). Its integration with a “tunable curved waveguide” (TCWG) and their actuation by a MEMS (micro electromechanical systems) electrostatic comb actuator are also designed for integrated photonic circuits. With this kind of structure, a widely and continuously tunable narrow-band resonance ranging up to 200 nm is achieved with a MEMS actuation voltage less than 70 V. Its applications in widely tunable photonic filters and lasers are promising.

©2012 Optical Society of America

OCIS codes: (130.7408) Wavelength filtering devices; (130.5296) Photonic crystal waveguides; (130.3120) Integrated optics devices; (230.5750) Resonators; (140.3948) Microcavity devices.

References and links

1. J. D. Joannopoulos, S. G. Johnson, J. N. Winn, and R. D. Meade, *Photonic Crystals: Molding the Flow of Light*, 2nd ed. (Princeton University Press, 2008).
2. K. J. Vahala, “Optical microcavities,” *Nature* **424**(6950), 839–846 (2003).
3. S. Fan, P. R. Villeneuve, J. D. Joannopoulos, and H. A. Haus, “Channel drop tunneling through localized states,” *Phys. Rev. Lett.* **80**(5), 960–963 (1998).
4. M. Belotti, M. Galli, D. Gerace, L. C. Andreani, G. Guizzetti, A. R. Md Zain, N. P. Johnson, M. Sorel, and R. M. De La Rue, “All-optical switching in silicon-on-insulator photonic wire nano-cavities,” *Opt. Express* **18**(2), 1450–1461 (2010).
5. D. Sridharan, R. Bose, H. Kim, G. S. Solomon, and E. Waks, “A reversibly tunable photonic crystal nanocavity laser using photochromic thin film,” *Opt. Express* **19**(6), 5551–5558 (2011).
6. I. W. Frank, P. B. Deotare, M. W. McCutcheon, and M. Lončar, “Programmable photonic crystal nanobeam cavities,” *Opt. Express* **18**(8), 8705–8712 (2010).
7. R. Perahia, J. D. Cohen, S. Meenehan, T. P. M. Alegre, and O. Painter, “Electrostatically tunable optomechanical “zipper” cavity laser,” *Appl. Phys. Lett.* **97**(19), 191112 (2010).
8. X. Chew, G. Zhou, H. Yu, F. S. Chau, J. Deng, Y. C. Loke, and X. Tang, “An in-plane nano-mechanics approach to achieve reversible resonance control of photonic crystal nanocavities,” *Opt. Express* **18**(21), 22232–22244 (2010).
9. G. Liang, C. Lee, and A. J. Danner, “Design of narrow band photonic filter with compact MEMS for tunable resonant wavelength ranging 100 nm,” *AIP Advances* **1**(4), 042171 (2011).
10. P. R. Villeneuve, J. S. Foresi, J. Ferrera, E. R. Thoen, G. Steinmeyer, S. Fan, J. D. Joannopoulos, L. C. Kimerling, H. I. Smith, and E. P. Ippen, “Photonic-bandgap microcavities in optical waveguides,” *Nature* **390**(6656), 143–145 (1997).
11. M. Y. Liu and S. Y. Chou, “High-modulation-depth and short-cavity-length silicon Fabry-Perot modulator with two grating Bragg reflectors,” *Appl. Phys. Lett.* **68**(2), 170–172 (1996).
12. B. Schmidt, Q. Xu, J. Shakya, S. Manipatruni, and M. Lipson, “Compact electro-optic modulator on silicon-on-insulator substrates using cavities with ultra-small modal volumes,” *Opt. Express* **15**(6), 3140–3148 (2007).
13. A. Taflove and S. C. Hagness, *Computational Electrodynamics: The Finite-Difference Time-Domain Method* (Artech, 2000).
14. A. F. Oskooi, D. Roundy, M. Ibanescu, P. Bermel, J. D. Joannopoulos, and S. G. Johnson, “Meep: A flexible free-software package for electromagnetic simulations by the FDTD method,” *Comput. Phys. Commun.* **181**(3), 687–702 (2010).
15. Y. Zhang, M. W. McCutcheon, I. B. Burgess, and M. Loncar, “Ultra-high-*Q* TE/TM dual-polarized photonic crystal nanocavities,” *Opt. Lett.* **34**(17), 2694–2696 (2009).
16. V. R. Almeida, Q. Xu, C. A. Barrios, and M. Lipson, “Guiding and confining light in void nanostructure,” *Opt. Lett.* **29**(11), 1209–1211 (2004).
17. C. O. M. S. O. L. Multiphysics, <http://www.comsol.com>.

1. Introduction

Photonic crystal-based optical micro-cavities [1, 2] have various applications such as optical filters [3], switches [4] and photonic crystal lasers [5]. When integrating such devices in photonic circuits, on-chip reconfiguration of the devices for programmable modulation of light is desirable. Recently widely and continuously tunable resonances ranging 10 to 100 nm have become an interesting research direction through the design of compact reconfigurable micro/nano photonic structures integrated with MEMS [6–9]. These designs are usually silicon photonic crystal based structures suspended in air. Due to the high refractive index contrast between the silicon waveguide to the air holes, the width of the photonic band gap can be more than 300 nm centered at the optical communication wavelength 1550 nm with a proper design geometry [10]. Though a tunable range for the resonance of up to 100 nm has been shown possible in our previous work [9], itself already 20 times wider than that achievable by carrier injection [11,12] and 5 to 10 times wider than that of any other reported MEMS electrostatic tuning designs [6–8], there is still available wavelength range within the photonic band gap to accommodate a wide (> 100 nm) tuning range for the narrow-band resonance, which would provide a wider range of signal channel selection for tunable optical filters, switches and photonic crystal lasers. In our previous design [9] employing a straight split photonic crystal resonator with a nano-meter wide air gap throughout the structure, the tuning range of resonance with narrow band width and high transmission could only achieve 100 nm, which is limited by the change of effective refractive index as the air gap becomes wider and wider in the course of modulation.

In this paper, we show that a very wide tuning range of up to 200 nm (which is twice as wide as ever reported previously for such a sharp resonance [9]) by proposing a new type of photonic resonator suspended in air, namely a “tunable curved resonator (TCR)”. To construct the TCR, a straight photonic resonator is curved at the cavity part and divided into two parts with one of them driven by a MEMS electrostatic comb actuator, providing the ability of tuning the length of a resonant cavity made of solid materials for efficiently tuning its resonant wavelength, which is not possible with straight cavities as discussed firstly in the paper. Then, in consideration of fabrication issues, we provide different designs for TCRs without or with an air gap. Finally, the integration of TCR in a photonic circuit via a “tunable curved waveguide” (TCWG) and actuation by MEMS are also designed.

2. Tuning a resonator with a straight cavity

In this section we discuss how one can tune the cavity length of a straight silicon (refractive index $n = 3.48$)/air photonic resonator suspended in air, as shown in Fig. 1(a). An intuitive way is to divide the structure from the center of the cavity (origin O) into two parts by an air break, as shown in Fig. 1(b), then the length of the cavity is tuned from C to $C + \Delta z$.

In this situation, the length of the cavity is increased by a low refractive index material (air for Δz) only, which means the length increment of the cavity is inefficient, and hence so is the tuning range of the resonance. Also because of this air break, there is no way to confine the highly localized electromagnetic field in the cavity region which will reduce the transmittance a lot. As can be seen from the transmission spectra in Fig. 1(c), $\Delta z = 0$ provides a highly transmitted (83%) resonant peak at 1524 nm within the photonic band gap (shown as inset of Fig. 1). However, when Δz becomes wider and wider, the transmittance becomes lower and lower (2% for $\Delta z = 100$, hardly useful) and the resonant wavelength can be shifted by 9 nm only. Simulations are performed with the three dimensional finite-difference time-domain (FDTD) method [13] and a freely available software package [14], using the TM-polarization as defined in Fig. 1(a). The transmittances are normalized to straight silicon ribs with thickness and width the same as the corresponding photonic resonators (same for the rest) surrounded by air. The structure of the photonic resonator has central inversion symmetry relative to the origin O when $\Delta z = 0$ nm. For the spectra in Fig. 1(c), the structural parameters used are the positions of the i th air hole ($i = 1,2,3,\dots$ counting from the one nearest to the

origin to positive z), $x_i = \{0,0,0,0,0,0\}$ nm, $z_i = \{155, 425, 757, 1137, 1470, 1765\}$ nm; their radii $r_i = \{60, 85, 110, 110, 85, 60\}$ nm, the width of the photonic wire $w = 500$ nm, and its thickness $t = 500$ nm. Hence, using an air break in straight resonator to tune the cavity length, like the one in Fig. 1(b), cannot provide a wide tuning range of the resonance with high transmission.

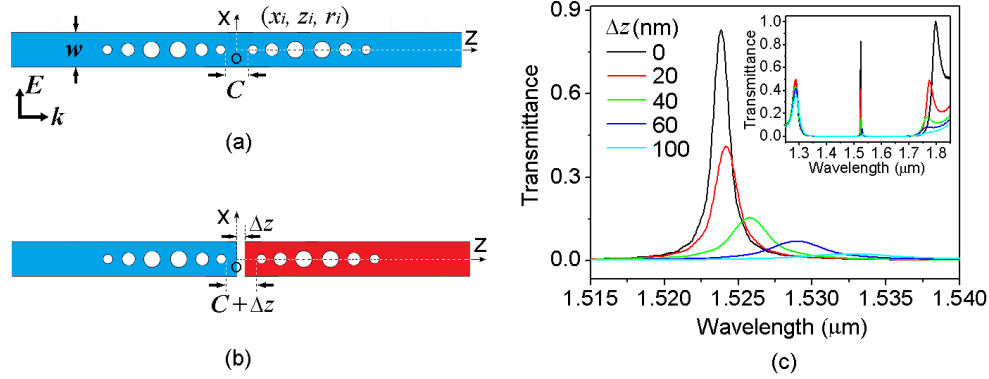


Fig. 1. (a) A straight photonic crystal resonator with cavity length C . (b) Tuning the length of the cavity by an air break introduced by shifting the red part along the z -direction by distance Δz . (c) Transmission spectra of the resonator as a function of Δz . The inset shows the position of the resonant peak relative to the wide photonic band gap.

3. TCR without an air gap

To avoid introducing an air break in the cavity region when shifting half of the resonator in the z -direction, we introduce the TCR (tunable curved resonator) design shown in Fig. 2(a). The blue and red parts are identical and have central inversion symmetry relative to origin O when $\Delta z = 0$. For each part, it is composed of a straight waveguide as the input or output port, and a curved part as the cavity, with air holes located along the curved structure. There is no gap between the blue and red parts in this design. For tuning the length of the cavity, the red part will be shifted in the z -direction along the dashed line at $x = 0$. Some corresponding structures after a shift are shown in Fig. 2(a), indicating the effective increase in length of the curved cavity and decrease in its width.

For the example in Fig. 2(a), the thickness of the structure $t = 500$ nm, the width of the input and output ports are $w = 450$ nm, and the edge of the curved waveguide are composed of two circumference segments AB and BA' from two circles with the same radii of 5330 nm and centered at $(x_i, z_i) = (-2220, -940)$ nm and $(2680, 1150)$ nm respectively. The positions of the air holes embedded in the red part are $x_i = \{-50, -145, -205, -225, -225, -225\}$ nm, $z_i = \{57, 301, 624, 1017, 1360, 1664\}$ nm when $\Delta z = 0$, and their radii are $r_i = \{50, 75, 100, 100, 75, 50\}$ nm. These values are optimized locally for relatively high transmission throughout the whole tuning range. As shown in Fig. 2(b), when the red part is shifted from $\Delta z = 0$ to 235 nm, the resonant wavelength shifts from 1423 nm to 1625 nm, ranging 202 nm, and the transmittance is more than 68%. The full width half maximum (FWHM) and the quality factor (Q) of the resonant peaks are shown in Fig. 2(c). The widening in the FWHM and decreasing in Q of the peak when it shifts from the middle of the band gap to the band edge is because of the reduction in reflection of the band gap. Figure 2(d) shows the mode profile of the resonant peak when $\Delta z = 75$ nm as a typical example. It shows that there is strong localization of resonance along the curved cavity of the resonator by the confinement from photonic band gap and total internal reflection, and the light field is also well confined in both of the straight input and output ports. This shows the feasibility of using the curved photonic resonator for wide tunability of resonant wavelength and its integration with photonic circuits. A narrower resonant peak can be obtained by increasing the number of air holes; while higher

transmission can be obtained by universally optimizing the size and the positions of the air holes and the curvature of the curved cavity.

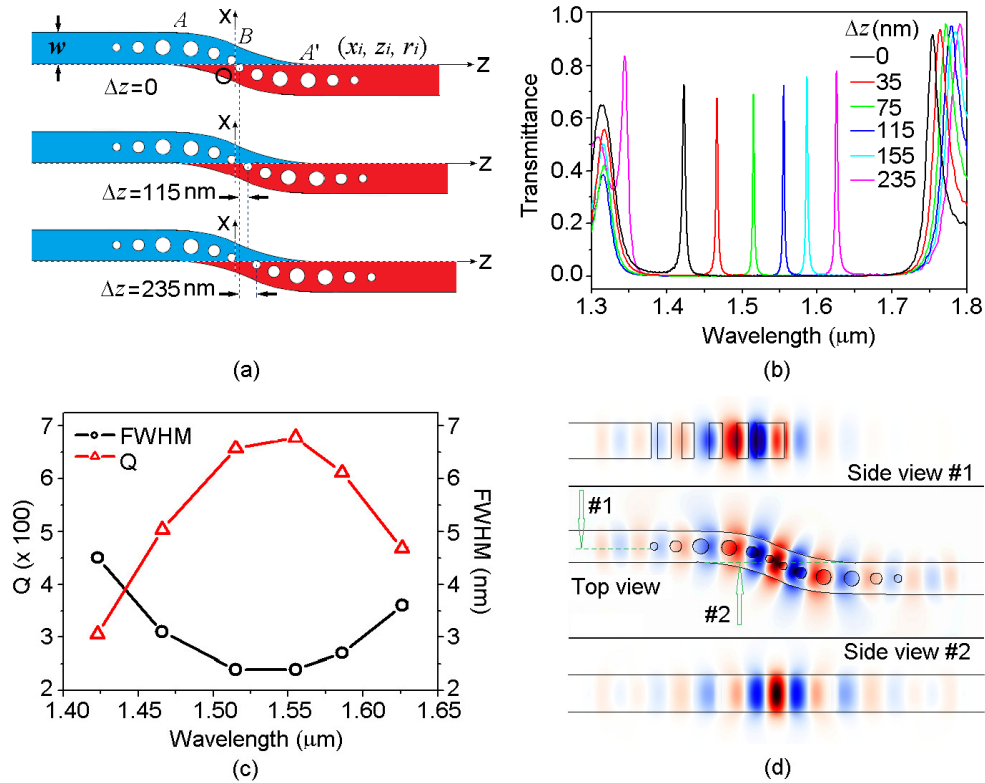


Fig. 2. (a) A design of a tunable curved photonic resonator without an air gap between the blue and red parts. The red part can be shifted in z -direction. Two examples for $\Delta z = 115$ and 235 nm are shown. (b) Transmission spectra of the resonator as a function of Δz . The wavelength of the resonant peak can be tuned ranging 202 nm. (c) FWHM and Q factor of the resonant peaks throughout the tuning range. (d) A typical mode profile when $\Delta z = 75$ nm showing confinement of the light field by the curved photonic resonator.

4. TCR with an air gap

Now we consider when an air gap is introduced between the blue and red parts which is inevitable in fabrication, and how to accommodate the impact of such gap to achieve widely tunable and highly transmitted resonant performance in the design stage.

We still use the TM-polarization as defined in Fig. 1(a); this is because TM-polarization is favored for high-transmission and narrow-band resonance when using planar photonic crystal platforms based on thin semiconductor slabs perforated with a lattice of holes [15].

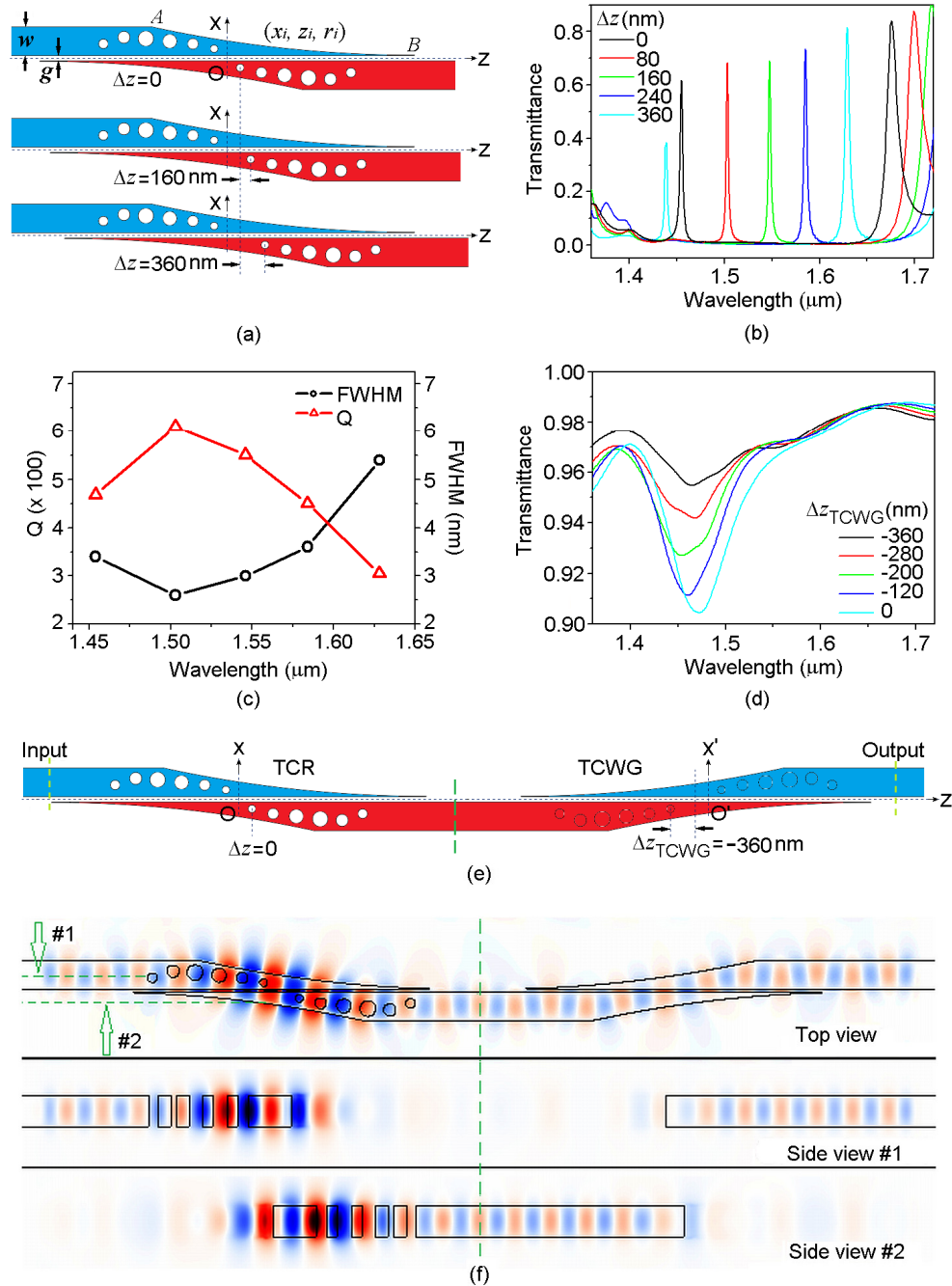


Fig. 3. (a) A design for a tunable curved resonator (TCR) with an air gap between the blue and red parts. The red part will be shifted in the z -direction. Two examples for $\Delta z = 160$ and 360 nm are shown. (b) Transmission spectra of the TCR as a function of Δz . The wavelength of the resonant peak can be tuned ranging 175 nm. (c) FWHM and Q factor of the resonant peaks in (b) in the tuning range. (d) Transmission spectra of the TCWG using $\Delta z_{\text{TCWG}} = -360, -280, -200, -120$ and 0 nm as examples for $\Delta z = 0, 80, 160, 240$ and 360 nm in Fig. 3(b), respectively. (e) Integration of structure TCR with TCWG for connection to external photonic circuit providing the Input and Output ports. (f) Mode profile for the structure in (e) using $\Delta z = 160$ nm as an example.

If an air gap (g) with width of tens of nano-meters is introduced between the blue and red waveguides, as shown in Fig. 3(a), the TM-polarized light field will have most of its intensity localized and guided by the air gap because of the high contrast index-discontinuity [16]. When the air gap is short in the z -direction, e.g., for Fig. 2(a), if we just shift the red part in the negative x -direction to introduce an air gap, because the curvatures of circumference segments AB and BA' are large (radii as small as about 5000 nm), which means the length of the air gap covers only the curved cavity region, the localized resonant energy in the cavity will leak through the openings of the air gap in the z -direction to air, resulting in very low transmittance in the output port (calculated but not shown here).

For high transmission, we should design an air gap much longer than the length of the curved cavity region, so that light leakage will not happen around the cavity region to such an extent. We introduce the design shown in Fig. 3(a) as an example, the thickness of the structure $t = 500$ nm, the width of the input and output ports are $w = 450$ nm. Comparing to Fig. 2(a), the difference is that there is an air gap with width $g = 20$ nm (width of the gap plotted not to scale in Fig. 3(a) and 3(e)) between the blue and red parts; and we use a long circumference segment AB from a circle with large radius of $19 \mu\text{m}$ and centered at $(x, z) = (19030, 2880)$ nm, which forms an long air gap extending throughout the whole structure. The long tail of the segment resulting from the large radius can gradually and effectively transfer the energy of the light field from the blue part to the red part across the air gap, as shown in the left part of Fig. 3(f) using $\Delta z = 160$ nm as an example. The positions of the air holes in the red part of the waveguide in Fig. 3(a) for $\Delta z = 0$ are $x_i = \{-120, -195, -235, -275, -295, -215\}$ nm, $z_i = \{135, 449, 804, 1210, 1565, 1880\}$ nm, and their radii are $r_i = \{50, 75, 100, 110, 80, 60\}$ nm. They are put along a curve style for guiding the wave front of the mode profile likely perpendicular to the edge of the waveguide as shown in the left part of the “top view” panel in Fig. 3(f) for better confinement by total internal reflection and hence higher transmission throughout the tuning range as shown in Fig. 3(b). Figure 3(b) shows that when the red part is shifted from $\Delta z = 0$ to 360 nm (some of the corresponding structure after the shift is shown in Fig. 3(a)) the resonant wavelength shifts from 1454 nm to 1629 nm, ranging 175 nm, and the transmittance is more than 62%. The FWHM and Q factor of the resonant peaks are shown in Fig. 3(c), having a similar varying trend as in Fig. 2(c). Because the long air gap reduces the contrast of the effective refractive index throughout the TCR structure, including the curved cavity region, narrower band gap and longer shift of the structural component in z -direction result as compared to the example in Fig. 2. Nevertheless, it is promising to further optimize the TCR structure with an air gap to achieve performance as good as the one without an air gap, which will be studied after this conceptual paper.

5. Integration with TCWG and actuation by MEMS

For connection with an external photonic circuit providing the Input and Output ports, we construct an integrated tunable structure TCR + TCWG as shown in Fig. 3(e): first remove all the air holes in the TCR with $\Delta z = 360$ nm in Fig. 3(a) and flip it horizontally to form a TCWG, as shown in the right part of Fig. 3(e) with origin O' ; the circles from the original TCR are for guidance of visualization purposes only; then this TCWG is connected to the TCR with $\Delta z = 0$ nm as shown in the left part of Fig. 3(e) with origin O . The joined waveguide in red in Fig. 3(e) is tunable in the z -direction, and the displacement between the two waveguides forming the TCWG Δz_{TCWG} changes from -360 to 0 nm accordingly when Δz changes from 0 to 360 nm. Figure 3(d) shows the transmittance of the TCWGs. It shows that the transmittance of the TCWG is higher than 95% when using $\Delta z_{\text{TCWG}} = -360, -280, -200, -120$ and 0 nm as examples for $\Delta z = 0, 80, 160, 240$ and 360 nm in Fig. 3(b), respectively. So the coupling loss between the TCR and the Output port by the TCWG is low. Figure 3(f) shows the whole mode profile from the Input port to the TCR (left part of Fig. 3(f)), then coupled out via a TCWG (right part of Fig. 3(f)) to the Output port, using $\Delta z = 160$ nm as an example.

For actuation by MEMS, we fix the Input and Output ports in Fig. 3(e) and attach the tunable part in the TCR + TCWG shown as red in Fig. 3(e), to a designed MEMS electrostatic comb actuator for its shifting in the z-direction, as shown in Fig. 4. Finite element analysis [17] with Young's modulus (170 GPa) and Poisson's ratio (0.28) of crystalline silicon is used to simulate the MEMS actuation. By calculation, the x-displacement of the tunable part is less than 0.5 nm throughout the whole range of applied actuation voltage, so the shift is nearly only in the z-direction which is consistent with the working principle of the designed tunable photonic circuit (TCR + TCWG). A shift by $\Delta z = 360$ nm is shown by the enlarged view for the TCR part in Fig. 4, and a similar view can be seen for the TCWG part. The actuation voltage needed is less than 70 V for Δz from 0 to 360 nm, as shown in the inset of Fig. 4.

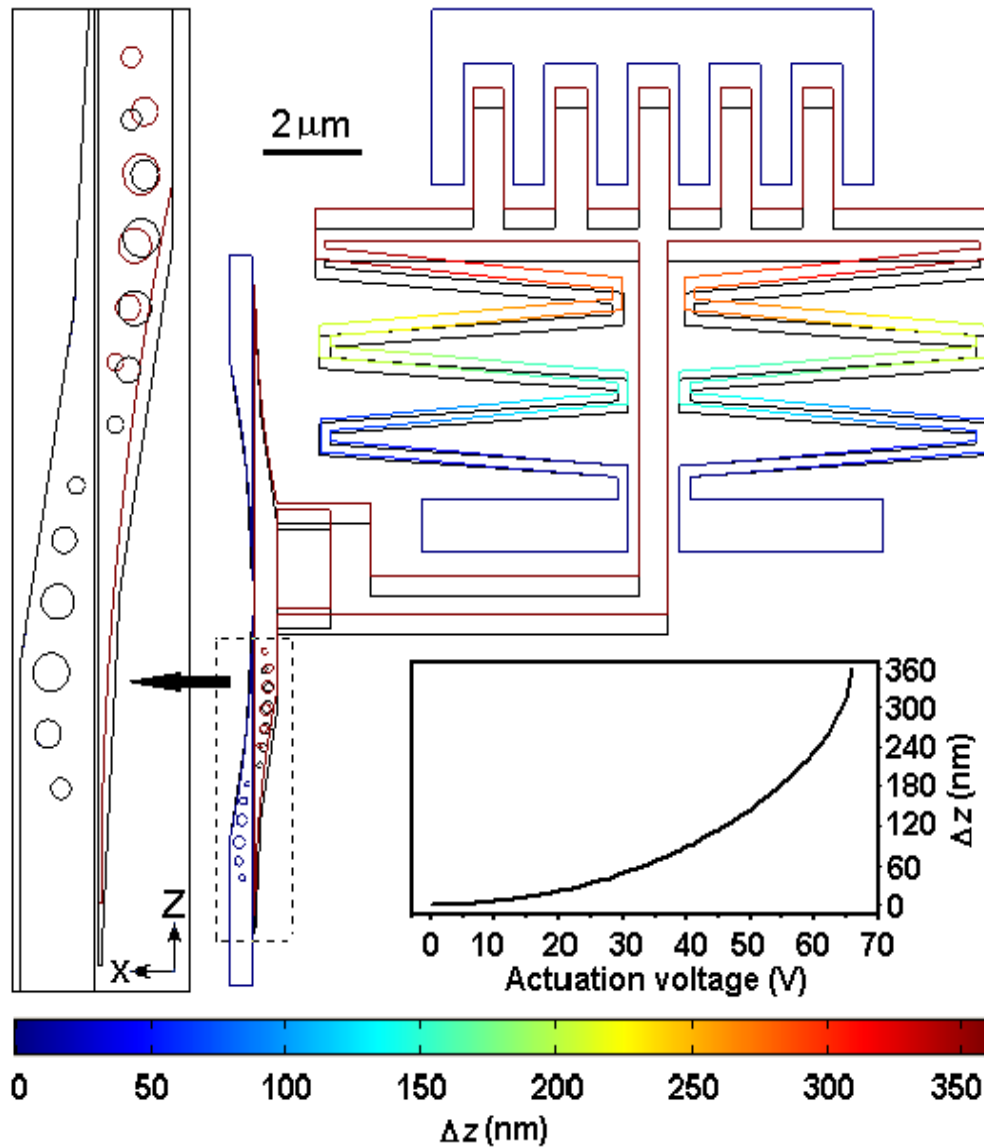


Fig. 4. Actuation for the integrated photonic circuit (TCR + TCWG) by a MEMS electrostatic comb actuator. An enlarged view of the dashed squared area shows $\Delta z = 360$ nm for the tunable part of the TCR. Δz as a function of the actuation voltage is shown in the inset.

The above design ideas for the integrating a TCR having an air gap with TCWG and MEMS actuator can also be applied to a TCR without an air gap (Fig. 2) for a resonance tuning range of up to 202 nm. A wider tuning range is possible by further optimizing the photonic structures.

6. Discussion

For the examples in Fig. 2 and Fig. 3, we just demonstrate the design concept for wide tunability by simple structure. We further investigate how high the Q factor can be increased to by simply adding N more periodic holes to the structure. For an example shown in Fig. 5(a), we use the same z -distance between the original holes #3 and #4, and the same size and x -position as the original hole #4 as in Fig. 2(a) for the N more holes. The Q factor as a function of N is shown in Fig. 5(b). As $N > 5$, the Q factor for each sampled resonance saturates at about 2500 to 5000, which is about 5 to 10 times as high as those in Fig. 2(c).

The curved cavity is a kind of transformation of straight cavity, and they share the same physics as the Fabry-Perot resonator. However, the curved cavity introduces more scattering loss than straight cavity because the wave vector is not strictly parallel to the waveguide at the curvatures. The Q factor from straight resonator without optimized structure saturates at $\sim 10^4$ [18], and be improved to $\sim 10^5$ after optimization [4]. The Q factor from the curved resonator in this paper is achievable at least up to $\sim 5 \times 10^3$ without optimization (Fig. 5(b)), so it is promising to have it approaching $\sim 10^4$ by further optimization for applications. The Q factor of the curved cavity which will be about one order less than straight cavity has been compensated for achieving high tuning range for the resonant wavelength.

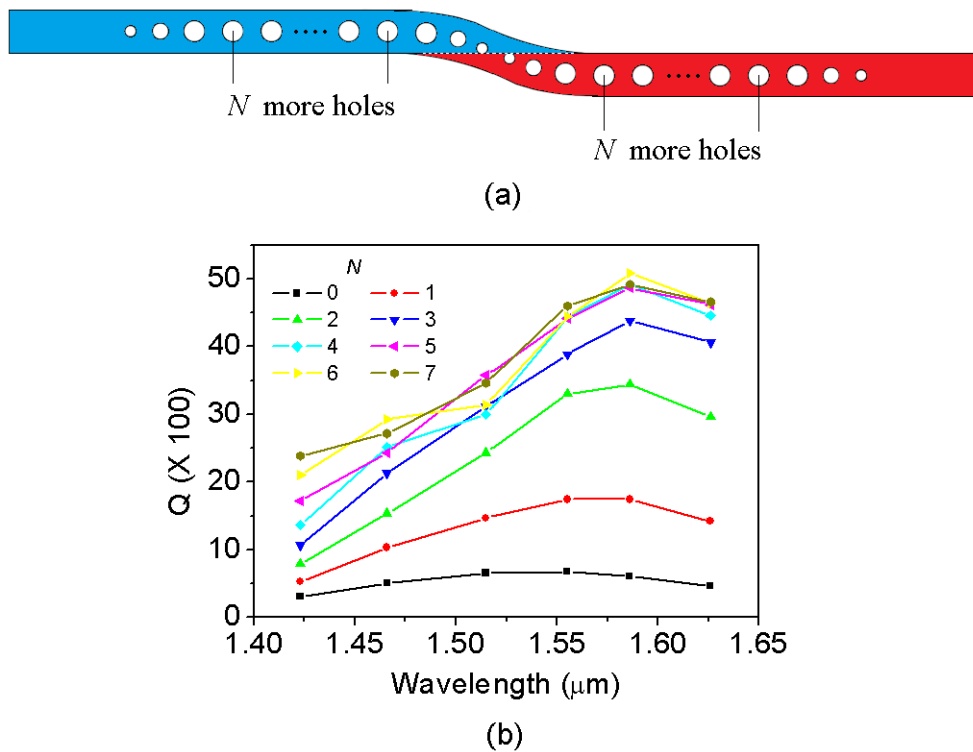


Fig. 5. (a) Adding N more air holes in the photonic structure in Fig. 2(a) for increasing the Q factor of the curved cavity. (b) Q factor as a function of the number of added holes N , showing saturation of Q factor when $N > 5$.

7. Conclusion

In conclusion, we have proposed a kind of photonic resonator—tunable curved resonator (TCR)—for efficiently tuning the optical length of a resonant cavity made of a solid material. Its integration with a tunable curved waveguide (TCWG) for coupling with external photonic circuits and their actuation by MEMS electrostatic comb actuator are also designed. With this kind of structure, a widely and continuously tunable narrow-band resonance ranging up to 200 nm is achieved with a MEMS actuation voltage less than 70 V. Its applications in widely and continuously tunable nano-photonic filtering and lasing are promising.

Acknowledgments

This work was supported in part by Singapore's A*Star Science and Engineering Research Council (SERC) grant 0921010049.